Title

Correlated scanning Kelvin probe and conductive atomic force microscopy studies of dislocations in gallium nitride

Journal

Journal of Applied Physics, 94(3)

ISSN

0021-8979

Authors

Simpkins, B S
Yu, E T
Waltereit, P
et al.

Publication Date

2003-08-01

Peer reviewed

Correlated scanning Kelvin probe and conductive atomic force microscopy studies of dislocations in gallium nitride

B. S. Simpkins and E. T. Yu[a)]
Department of Electrical and Computer Engineering and Program in Materials Science and Engineering, University of California at San Diego, La Jolla, California 92093-0407

P. Waltereit and J. S. Speck
Department of Materials, University of California, Santa Barbara, Santa Barbara, California

(Received 14 October 2002; accepted 2 May 2003)

Scanning Kelvin probe microscopy (SKPM) and conductive atomic force microscopy (C-AFM) have been used to image surfaces of GaN grown by molecular beam epitaxy. Detailed analysis of the same area using both techniques allowed imaging and comparison of both surface potential variations arising from the presence of negatively charged threading dislocations and localized current leakage paths associated with dislocations. Correlations between the charge state of dislocations, conductivity of current leakage paths, and dislocation type were thereby established. Analysis of correlated SKPM and C-AFM images revealed a density of negatively charged features of $\sim 3\times 10^{8}$ cm^{-2} and a localized current leakage path density of $\sim 3\times 10^{7}$ cm^{-2}, with approximately 25% of the leakage paths spatially correlated with negatively charged dislocation features. Based on correlated topography and previous studies quantifying the densities of edge, screw, and mixed dislocations, our results suggested that dislocations having an edge component behave as though negatively charged while pure screw dislocations are solely responsible for the observed leakage paths and are uncharged. © *2003 American Institute of Physics.*
[DOI: 10.1063/1.1586952]

I. INTRODUCTION

Group III–nitride semiconductors have been the subject of intensive research in recent years for both optoelectronic applications and high-power, high-speed electronic devices.[1,2] Although dramatic progress has been made in improving both epitaxial material quality and device performance, substantial challenges remain. In particular, the lack of readily available homoepitaxial substrates typically necessitates growth on either sapphire or SiC, both of which lead to degradation in material quality predominantly through the presence of high densities of threading dislocations. Threading dislocations in GaN degrade device performance through carrier scattering,[3] nonradiative recombination,[4] and increased reverse-bias leakage current.[5,6] However, the correlations among dislocation type, electronic properties such as charge and conductivity, and corresponding effects on device performance remain subjects of active investigation.

The presence of threading dislocations can often be determined from the surface topography of GaN epitaxial layers, as surface pits can be an indication of the surface termination of threading dislocations.[7] These topographic dislocation markers have been correlated with the presence of negative charge using scanning Kelvin probe microscopy (SKPM) on both AlGaN/GaN heterostructures grown by molecular beam epitaxy[8] (MBE) and GaN grown by metalorganic chemical vapor deposition[9] (MOCVD). Negatively charged dislocations have also been imaged using scanning capacitance microscopy on MOCVD-grown GaN on sapphire[10] and MOCVD-grown AlGaN/GaN heterojunction field effect transistor (HFET) structures on SiC;[11] however, the precise crystallographic nature of these negatively charged dislocations was not determined. Pure screw dislocations have been implicated as the source of localized reverse bias current leakage paths;[5] however, the charge state of these leakage paths and their correlation with the negatively charged dislocations observed in prior studies has yet to be reported. Understanding the relationship between dislocation-related leakage paths and negatively charged dislocations is necessary in order to correlate device degradation mechanisms with specific dislocation types. In this respect, the results of the current study will help determine which dislocation types are most harmful to device performance and will contribute to a more complete characterization of threading dislocations in GaN.

II. EXPERIMENTAL METHODS

In the present work, MBE was used to deposit GaN layers on GaN templates grown by MOCVD on sapphire substrates. The MOCVD templates are produced with thin low-temperature GaN nucleation layers followed by $\sim 2\ \mu$m of GaN grown at high temperature. A ~ 350 nm GaN layer was then grown by MBE in the gallium droplet regime near the crossover in V:III ratio between Ga-droplet formation and no Ga- droplet formation. Further details of the growth conditions and procedures are described elsewhere.[12] Previous studies by transmission electron microscopy[13] (TEM) have indicated that total dislocation densities of $\sim 1\times 10^{9}$ cm^{-2} are typical for these MOCVD templates, consisting of pure edge dislocation densities of $(0.5-1)\times 10^{9}$ cm^{-2} and screw-

a)Electronic mail: ety@ece.ucsd.edu

component dislocation densities of $\sim 5\times 10^8$ cm^{-2} with the majority being of mixed character. The MBE films grown on the MOCVD templates have been shown to retain the defect structure and density of the template.[12]

Samples used in our studies were stored in ambient conditions and then cleaned with trichloroethylene, acetone, and isopropanol in an ultrasonic bath prior to examination. Ohmic contacts were fabricated by deposition of Al/Ti metallization and subsequent rapid thermal annealing in H_2/N_2 at 650 °C for 1 min. Atomic force microscopy (AFM), SKPM, and conductive atomic force microscopy (C-AFM) data were obtained in a Digital Instruments Nanoscope IIIa MultiMode microscope under ambient conditions ($\sim$20 °C with 50% humidity). Co/Cr and conductive diamond coated tips were used for the SKPM and C-AFM experiments, respectively.

To acquire AFM and SKPM images, a topographic line scan is first obtained by AFM using TAPPINGMODE imaging, and then that same line is rescanned in LIFTMODE with the tip raised to a lift height of $\sim$30 nm. The basic principles of SKPM have been described in detail elsewhere.[14,15] In brief, SKPM is used to image variations in the contact potential difference $\Delta\phi$ between a conducting probe tip and the sample under investigation; $\Delta\phi$ is defined[16] as $(\phi_{\text{tip}} - \phi_{\text{GaN}})/q$, where ϕ_{tip} and ϕ_{GaN} are the work functions of the tip and sample, respectively and q is the magnitude of the electron charge. In this experiment, a bias voltage $V_{\text{tip}} = V_{\text{dc}} + V_{\text{ac}} \sin \omega t$ is applied directly to the tip, holding the sample at ground potential, where ω is the tip resonant frequency. A feedback loop continually adjusts V_{dc} to maintain a condition that minimizes the force component at frequency ω between the tip and sample and is recorded as a function of position, yielding a map of the sample surface potential. Features in the SKPM image can then be related to changes in the surface Fermi level position caused by the presence of charged defects.

The C-AFM procedures employed in our studies have been described previously.[5] Briefly, a conductive tip is kept in constant contact with the surface by scanning in contact mode and acts as a Schottky contact to our sample. A reverse-bias condition is established through the application of a positive bias (+12 V in this experiment) to an Ohmic contact on the sample while the current through the tip is measured with a current amplifier. The current through the tip is measured simultaneously with topography and is recorded as a function of tip position; the resulting current images reveal nonuniformities in sample conductivity. The specific features of interest in this work are localized, highly conductive current leakage paths associated with threading dislocations.[5,6]

III. RESULTS AND DISCUSSION

The presentation and discussion of our experimental results is divided into four sections. Section III A discusses the general characteristics of topographic, surface potential, and C-AFM results and the densities of pertinent features revealed using each method. Next, higher-resolution images are used in Sec. III B to establish that pure edge dislocations exhibit negatively charged surface potential features. Section III C examines the correlation between growth hillocks and SKPM measurements, indicating that a subset of screw-component dislocations, most likely mixed dislocations, also exhibit negatively charged surface potential features. Finally, Sec. III D examines the lack of spatial correlation between charged and conductive dislocations, demonstrating that these features have different origins, and also includes a summary of the results.

A. Charged and conductive features

Figure 1 shows representative images of (a) surface topography, (b) surface potential, and (c) reverse-bias current for a single 3×3 μm^2 area of the sample. The sample topography exhibited atomic terraces with a measured height of $\sim$0.3 nm, in close agreement with the 0.26 nm bilayer spacing of GaN. The intersection of a screw-component dislocation with the film surface creates an atomic step termination that may lead to spiral step procession and hillock formation[17] during growth under the conditions used.[7] Although inversion domains have also been reported at the cores of hillocks,[18] TEM studies[13] show that all inversion domains in the current samples terminate within the first 500 nm of MOCVD film growth. Spiral growth hillocks, with depressions located at the top, are clearly visible in Fig. 1(a), and other scanned areas, at a density of $\sim 3\times 10^8$ cm^{-2}—in agreement with the expected density of screw-component dislocations in these samples.[13] Small pits located away from the hillock peaks, several of which are visible in the upper right portion of Fig. 1(a), are examined and discussed in detail in Sec. III B.

Dark features, 10–20 mV in amplitude, are visible in the surface potential map of Fig. 1(b) and correspond to regions where the surface Fermi level is positioned closer to the valence band.[19] This Fermi level shift is consistent with the presence of negative charge in the dark regions of Fig. 1(b) and has previously been associated with negatively charged dislocations in GaN.[8,9,20] A detailed examination of this and other surface potential images for this sample yielded an approximate density of such negatively charged features of $\sim 3\times 10^8$ cm^{-2}; however, the true density may be higher due to feature overlap. Although the surface potential variations observed in the current work were somewhat smaller than those observed in previous studies, it should be noted that surface contamination and surface state charges may act to partially screen the potential associated with a charged dislocation, thereby decreasing the measured potential shift. The effect of surface treatment on the measured dislocation-induced potential has been investigated[21] and screening of dislocation-induced potentials by surface charges has been shown. While surface charge may be present and partially screening the potential variations measured in the present work, measured surface potential features were still 5–10 times the noise level of the instrument ($\sim$1 mV). Therefore, regions of decreased surface potential can be confidently associated with the presence of negative charge. As is demonstrated in Secs. III B and III C, these surface features are likely indicative of negatively charged bulk dislocation properties.

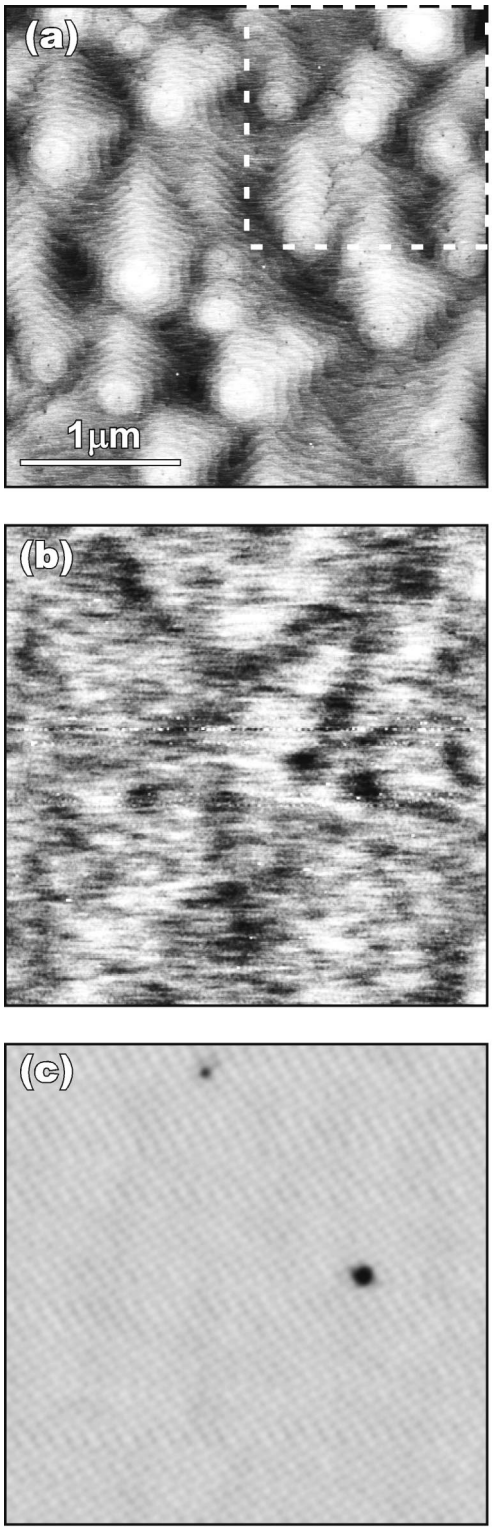

FIG. 1. (a) AFM topography, (b) surface potential, and (c) current maps corresponding to the same $3\times3\ \mu m^2$ area. The gray scales correspond to a range of 4 nm for topography, 25 mV for surface potential, and 10^{-11} A for the current map.

The two dark features in Fig. 1(c) correspond to highly conductive localized reverse-bias leakage paths. Analysis of several larger scanned areas yields a leakage path density of $\sim3\times10^7\ cm^{-2}$. Such reverse-bias leakage paths in GaN have been postulated to be associated with pure screw dislocations[5] and are the primary sources for reverse-bias leakage current in MBE-grown GaN.[6]

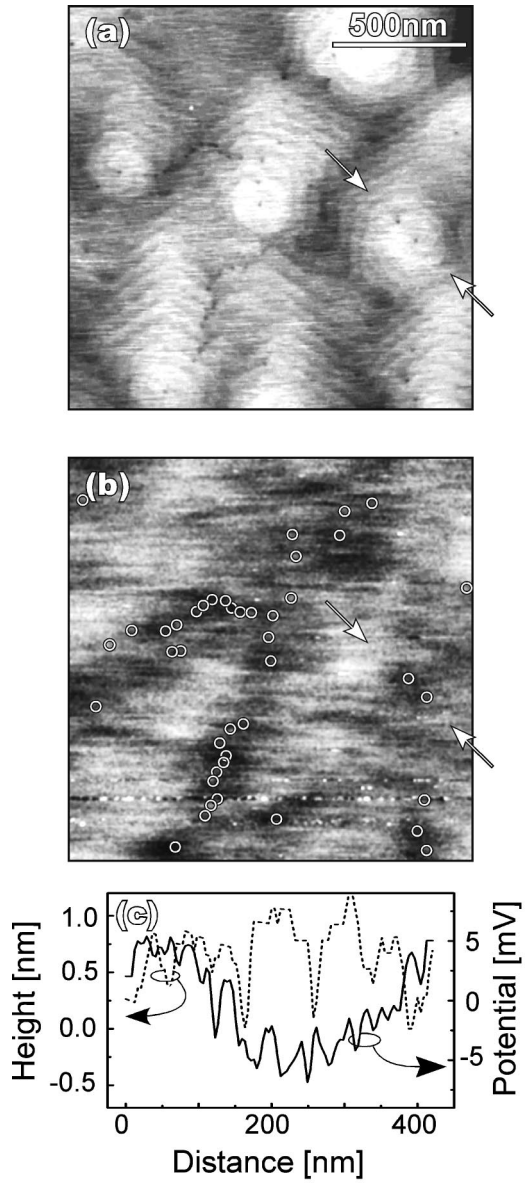

FIG. 2. (a) AFM topography and (b) surface potential maps of a $1.5\times1.5\ \mu m^2$ area with the locations of dislocation pits indicated by circles. (c) Dual section profile taken through two dislocations along the line indicated by arrows in (a) and (b). Gray scales correspond to 3 nm for topography and 25 mV for surface potential.

B. Electronic properties of pure edge dislocations

The correlation between the surface potential variations observed in Fig. 1(b) and threading dislocations is established in Fig. 2. Topographic and surface potential images of a $1.5\times1.5\ \mu m^2$ area are shown in Figs. 2(a) and 2(b), respectively. This area corresponds to the upper right quadrant of Fig. 1(a), indicated by the dashed box. Surface pits such as those seen in Fig. 2(a) have been shown to be associated with threading dislocations[7] and are commonly used as indicators of dislocations.[8–10] Pits at the center of a spiral growth hillock are expected to have a screw component while dislocation pits located away from hillock peaks and showing no

terminated steps are of pure edge character.[7] Open circles in Fig. 2(b) indicate the surface pits visible in the topographic image of Fig. 2(a). The clear coincidence between the dislocation-related pits and regions of decreased surface potential is evident in Fig. 2(b). The majority of dislocations in this material are of pure edge character,[13] and we associate these with the surface pits located away from hillock peaks. The density of these small pits located away from hillock peaks was $\sim 10^9$ cm^{-2}, in agreement with the expected pure edge dislocation density determined by TEM examination.[13] The strong correlation between topographic features associated with pure edge dislocations and areas of decreased surface potential, as demonstrated in Fig. 2(b), suggests that pure edge dislocations are negatively charged.[8,9] We have also observed a correlation between pits that occur at growth hillock peaks, corresponding to screw-component dislocations, and regions of decreased surface potential. These results indicate that the screw-component dislocations found in this region are negatively charged as well; however, this small region may not contain both mixed and pure screw dislocations, and analysis of larger areas will be presented in Secs. III C and III D.

A number of theoretical studies predict the presence of negative charge located at the core of edge dislocations.[22] And although early theoretical work predicted that both screw and edge dislocations should be electrically inactive,[23] subsequent simulations considering doping as well as growth conditions[22] and the presence of impurity defect complexes[24] do predict that acceptor-type defects can be present at the core of edge dislocations, leading edge dislocations to become negatively charged in *n*-type GaN. A section profile of topography and surface potential along the direction indicated by the arrows in Figs. 2(a) and 2(b) is shown in Fig. 2(c). The topographic and potential data are represented by the dotted and solid curves, respectively. The profile includes a pit located at a hillock peak and another located away from the peak. Each of the two dislocation pits is ~ 1 nm deep and ~ 50 nm wide. Along with reinforcing the correlation between the dislocations and the surface potential feature, Fig. 2(c) gives a clear quantitative measure of this surface potential depression (~ 12 mV).

C. Electrical properties of pure screw and mixed dislocations

Further insight regarding the crystallographic nature of charged dislocations comes by examining the correlation between the growth hillocks and surface potential variations in a larger, more statistically significant region. Figure 3 displays (a) topographic and (b) SKPM data with squares indicating leakage path locations and circles indicating hillock peak positions in Fig. 3(b) for a 5×5 μm^2 region. Note that every leakage path coincides with a growth hillock, which grows spirally about a screw or mixed dislocation located at the center. However, only $\sim 10\%$ of growth hillocks (calculated from several larger images) exhibited current leakage. This is consistent with previous findings[5,6] and is also consistent with the proposal that these leakage paths occur only at pure screw dislocations.[5] Specifically, hillocks form around pure screw and mixed dislocations and this material

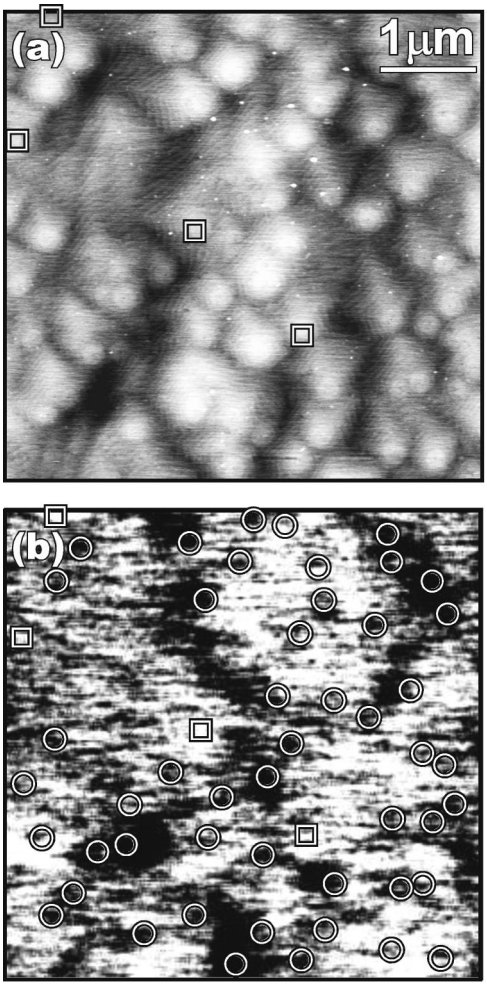

FIG. 3. (a) AFM topography and (b) surface potential maps of a 5 $\times 5$ μm^2 area with the locations of current leakage paths indicated by squares and locations of growth hillocks indicated by circles. Gray scales correspond to 5 nm for topography and 20 mV for surface potential.

contains about an order of magnitude more mixed than screw dislocations. It is therefore reasonable to postulate that $\sim 90\%$ of hillocks grow around mixed dislocations while the remaining 10% grow around pure screw dislocations; we further suggest, based on the previously reported association of current leakage paths with pure screw dislocations, that it is this 10% of hillocks associated with pure screw dislocations that exhibit current leakage.

Figure 3(b) shows a clear spatial correlation between nearly all of the hillock peaks, except those that exhibit leakage, and regions of reduced surface potential. This observation suggests that mixed dislocations, which should constitute $\sim 90\%$ of the hillock peaks, are negatively charged. The pronounced broad regions of decreased surface potential seen in Fig. 3(b) are most likely due to groupings of pure edge dislocations as was shown in Fig. 2(b). However, the topographic features associated with edge dislocations are too small to be visible in the image area shown in Fig. 3(a).

D. Correlation between charged and conductive dislocations

Our observations also demonstrate that negatively charged dislocations in GaN do not exhibit increased con-

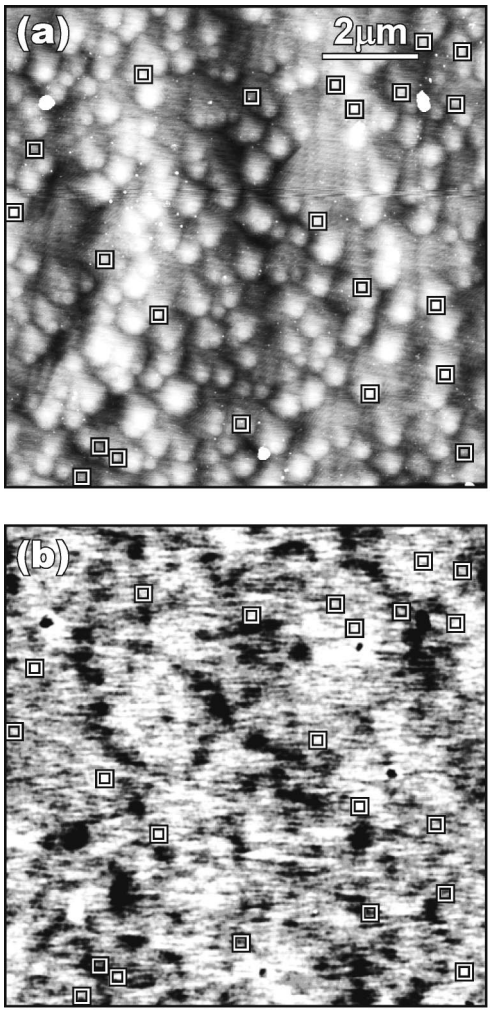

FIG. 4. (a) AFM topography and (b) surface potential maps of a 10 $\times 10\ \mu m^2$ area with the locations of current leakage paths indicated by squares, demonstrating the lack of correlation between leakage paths and negatively charged features. Gray scales correspond to 8 nm for topography and 25 mV for surface potential.

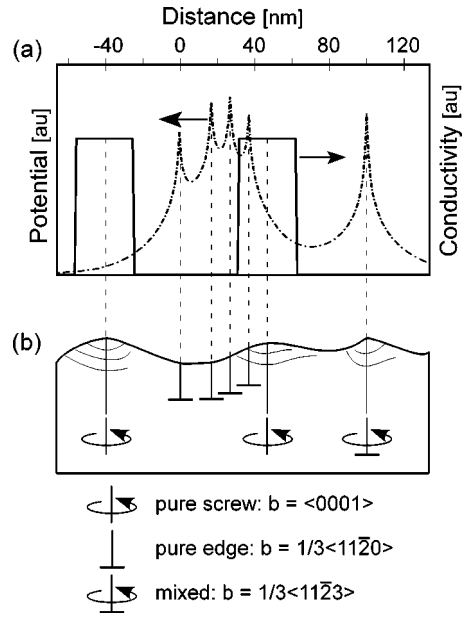

FIG. 5. Schematic illustration of various dislocation types and their respective electrical behaviors. (a) Electronic potential (dotted curve) and conductivity (solid black line) associated with dislocation and (b) schematic illustration of dislocation types, associated topography, and correspondence with electronic behavior shown in (a).

ductivity. By combining information in SKPM and C-AFM images, which reveal negatively charged dislocations and local current leakage paths, respectively, the spatial correlation between these features may be examined. Figure 4 shows (a) topographic and (b) surface potential images of a 10 $\times 10\ \mu m^2$ area with leakage path features, each represented by a square, overlaid onto the topographic and surface potential images. Recall that $\sim$10% of the spiral growth hillocks form around pure screws with the remaining $\sim$90% forming around mixed dislocations. As expected, $\sim$10% of growth hillocks exhibit current leakage, consistent with the postulate that only pure screw dislocations display this behavior. It may also be seen in the surface potential image of Fig. 4(b) that there is very little coincidence between the current leakage paths marked by squares and areas of decreased surface potential, indicated by dark SKPM contrast. Most of the leakage paths reside in bright regions in the SKPM map. An examination of this and other images reveals that only $\sim$25% of the leakage paths are spatially correlated with regions of decreased surface potential. The surface potential and leakage path feature densities, as well as the correlation percentages, are consistent over several scanned areas.

Given the area of decreased surface potential associated with a single negatively charged dislocation, approximately this level of overlap would be expected for random independent distributions of charged and conductive dislocations. More precisely, the measured surface potential features can be up to several hundred nanometers in size, making it plausible that an uncharged pure screw would be located within the range of the potential created by a neighboring, negatively charged edge or mixed dislocation. Assuming a dislocation-induced potential feature radius of 200 nm and a negatively charged feature density of $3\times10^8\ cm^{-2}$, $\sim$35% of the surface area would show reduced surface potential. It is therefore reasonable to assume that approximately this percentage of pure screws, if randomly distributed, will be located within these potential features. The lack of correlation between the negatively charged features and the leakage paths demonstrates that these features have distinctly separate origins. Based on previous and the current work indicating that only pure screw dislocations exhibit current leakage, combined with the lack of correlation between conductive and charged dislocations seen here, it is proposed that the highly conductive pure screw dislocations are uncharged.

Figure 5 summarizes our findings. Figure 5(a) illustrates the electronic behavior (electronic potential and conductivity) of the dislocations schematically represented in Fig. 5(b). The potential profile, shown as the dotted curve, is generated by summing potentials for the individual edge and mixed dislocations, presumed to be negatively charged and modeled according to Ref. 20, and is intended as a schematic illustration. The sign of the potential features has been in-

verted for comparative purposes; in addition, actual measured potential shifts will appear spatially larger than those plotted here due to the finite probe tip size and the tip-sample separation during the measurement. The conductivity behavior, plotted as a solid black line, assumes a steplike change with enhanced conductivity in the vicinity of a pure screw dislocation over an area equal to the size of the probe tip (~30 nm). Figure 5 thus shows the negatively charged behavior we attribute to pure edge and mixed dislocations, while also illustrating the highly conductive and uncharged behavior associated with pure screw dislocations. The figure also shows an uncharged screw dislocation located within the lateral range of a potential feature that is due to a nearby charged dislocation(s).

IV. CONCLUSION

In summary, we have studied the electrical behavior, specifically the charge state and conductivity, of edge, screw, and mixed dislocations in GaN. Spatially resolved and correlated measurements of topography, surface potential, and leakage current, indicate that the negatively charged threading dislocations present in GaN are not responsible for producing localized current leakage paths. Pure edge and mixed dislocations appear to be negatively charged and not highly conductive, while dislocations of pure screw type are the source of localized leakage paths and show no measurable charge.

ACKNOWLEDGMENTS

Part of this work was supported by ONR (POLARIS MURI), by Raytheon Corporation, and by NSF (Award No. DMR0072912).

[1] S. Nakamura, M. Senoh, S. Nagahama, N. Iwasawa, T. Yamada, T. Matsushita, H. Kiyohu, and Y. Sguimoto, Jpn. J. Appl. Phys., Part 2 **35**, L74 (1996).
[2] Y. F. Wu, B. P. Keller, P. Fini, S. Keller, T. J. Jenkins, L. T. Kechias, S. P. Denbaars, and U. K. Mishra, IEEE Electron Device Lett. **19**, 50 (1998).
[3] H. M. Ng, D. Doppalapudi, T. D. Moustakas, N. G. Weimann, and L. F. Eastman, Appl. Phys. Lett. **73**, 821 (1998).
[4] T. Sugahara, H. Sato, M. Hao, Y. Naoi, S. Tottori, K. Yamashita, K. Nishino, L. T. Romano, and S. Sakai, Jpn. J. Appl. Phys., Part 2 **37**, L398 (1998).
[5] J. W. Hsu, M. J. Manfra, R. J. Molnar, B. Heying, and J. S. Speck, Appl. Phys. Lett. **81**, 79 (2002).
[6] E. J. Miller, D. M. Schaadt, E. T. Yu, C. Poblenz, C. Elsass, and J. S. Speck, J. Appl. Phys. **91**, 9821 (2002).
[7] B. Heying, E. J. Tarsa, C. R. Elsass, P. Fini, S. P. Denbaars, and J. S. Speck, J. Appl. Phys. **85**, 6470 (1999).
[8] J. W. Hsu, M. J. Manfra, D. V. Lang, K. W. Baldwin, L. N. Pfeiffer, and R. J. Molnar, J. Electron. Mater. **30**, 110 (2001).
[9] G. Koley, and M. G. Spencer, Appl. Phys. Lett. **78**, 2873 (2001).
[10] P. J. Hansen, Y. E. Strausser, A. N. Erickson, E. J. Tarsa, P. Kozodoy, E. G. Brazel, J. P. Ibbetson, U. Mishra, V. Narayanamurti, S. P. Denbaars, and J. S. Speck, Appl. Phys. Lett. **72**, 2247 (1998).
[11] D. M. Schaadt, E. J. Miller, E. T. Yu, and J. M. Redwing, Appl. Phys. Lett. **78**, 88 (2001).
[12] B. Heying, R. Averbeck, L. F. Chen, E. Haus, H. Riechert, and J. S. Speck, J. Appl. Phys. **88**, 1855 (2000).
[13] X. H. Wu, L. M. Brown, D. Kapolnek, S. Keller, B. Keller, S. P. Denbaars, and J. S. Speck, J. Appl. Phys. **80**, 3228 (1996).
[14] M. Nonnenmacher, M. P. O'Boyle, and H. K. Wickramasinghe, Appl. Phys. Lett. **58**, 2921 (1991).
[15] H. O. Jacobs, H. F. Knapp, S. Müller, and A. Stemmer, Ultramicroscopy **69**, 39 (1997).
[16] S. M. Sze, *Physics of Semiconductor Devices*, 2nd ed. (Wiley and Sons, New York, NY, 1981), p. 246.
[17] W. K. Burton, N. Cabrera, and F. C. Frank, Philos. Trans. R. Soc. London, Ser. A **243**, 299 (1951).
[18] V. Potin, P. Ruterana, and G. Nouet, Mater. Sci. Eng., B **59**, 173 (1999).
[19] F. Robin, H. Jacobs, O. Homan, A. Stemmer, and W. Bachtold, Appl. Phys. Lett. **76**, 2907 (2000).
[20] B. S. Simpkins, D. M. Schaadt, E. T. Yu, and R. J. Molnar, J. Appl. Phys. **91**, 9924 (2002).
[21] J. W. Hsu, H. M. Ng, A. M. Sergent, and S. N. G. Chu, Appl. Phys. Lett. **81**, 3579 (2002).
[22] A. F. Wright and U. Grossner, Appl. Phys. Lett. **73**, 2751 (1998).
[23] J. Elsner, R. Jones, P. K. Sitch, V. D. Porezag, M. Elstner, Th. Frauenheim, M. I. Heggie, S. Öberg, and P. R. Briddon, Phys. Rev. Lett. **79**, 3672 (1997).
[24] J. Elsner, R. Jones, M. I. Heggie, P. K. Sitch, M. Haugk, Th. Frauenheim, S. Öberg, and P. R. Briddon, Phys. Rev. B **58**, 12571 (1998).